High-performance Cu_6Sn_5 alloy electrocatalyst for formaldehyde oxidative dehydrogenation and bipolar hydrogen production

Xiaoyang Fu, Dongfang Cheng, Ao Zhang, Jingxuan Zhou, Sibo Wang, Chengzhang Wan, Xun Zhao, Jun Chen, Philippe Sautet, Yu Huang*, Xiangfeng Duan**

X. Fu, J. Zhou, S. Wang, C. Wan, Prof. P. Sautet and Prof. X. Duan
Department of Chemistry and Biochemistry
University of California
Los Angeles, CA 90095, USA
E-mail: sautet@ucla.edu
E-mail: xduan@chem.ucla.edu

D. Cheng, Prof. P. Sautet
Department of Chemical and Biomolecular Engineering
University of California
Los Angeles, CA 90095, USA
E-mail: sautet@ucla.edu

X. Fu, A. Zhang, C. Wan, and Prof. Y. Huang
Department of Materials Science and Engineering
University of California
Los Angeles, CA 90095, USA
E-mail: yhuang@seas.ucla.edu

X. Zhao, Prof. J. Chen
Department of Bioengineering
University of California
Los Angeles, CA 90095, USA

Keywords: aldehyde oxidative dehydrogenation, hydrogen production, Cu_6Sn_5 alloy, electrocatalysis, electrodeposition

Abstract

Aldehyde assisted water electrolysis offers an attractive pathway for energy-saving bipolar hydrogen production with combined faradaic efficiency of 200 % while converting formaldehyde into value-added formate. Herein we report the design and synthesis of noble metal free Cu_6Sn_5 alloy as a highly effective electrocatalyst for formaldehyde electro oxidative dehydrogenation, demonstrating an ultrahigh geometric current density of 915±46 mA/cm^2 at 0.4 V vs. reversible hydrogen electrode, outperforming many noble metal electrocatalysts reported previously. The formaldehyde assisted water electrolyser delivers 100 mA/cm^2 at an ultralow low cell voltage of 0.124 V, and a high current density of 486±20 mA/cm^2 at a cell voltage of 0.6 V without any iR compensation, and exhibit nearly 200 % faradaic efficiency for bipolar hydrogen production at 100 mA/cm^2 in 88-hour long-term operation. Density functional theory calculations further confirm the notably lowered barriers for dehydrogenation and Tafel steps on the Cu_6Sn_5 surface compared to Cu, underscoring its potential as a highly active catalyst.

1 Introduction

By replacing the anodic water oxidation reaction in conventional water electrolysis with the oxidation reactions of other alternative substrates (*e.g.,* alcohols,[1-2] hydrazine,[3] sulfide,[4] amine,[5] and urea,[6] etc.), hybrid water electrolysis substantially lowers voltage requirement and energy consumption for hydrogen production, while simultaneously enabling the removal of environmental pollutants or the generation of value-added products.[7-8] Among the various substrates, aldehydes have attracted increasing recent interest for their unique electro-oxidative dehydrogenation reaction at low overpotential (Equation 1), which, when combined with the cathodic hydrogen evolution reaction (HER, Equation 2), could lead to a combined 200% faradaic efficiency (FE) for bipolar hydrogen production with 1 mole H_2 production

upon 1 mole electron transfer through the external circuit (0.5 mole H_2 from cathode and anode, respectively).[9-10] Furthermore, this reaction could bring additional environmental benefits by converting formaldehyde (a common pollutants in certain industrial wastewater[11-12]) to formate (a value-added commodity chemical that is ~4-fold more expensive than formaldehyde according to the export price from China to US).[13]

$$RCHO + 2OH^- \rightarrow RCOO^- + H_2O + \frac{1}{2}H_2 + 1e^- \qquad \text{(Equation 1)}$$

$$H_2O + 1e^- \rightarrow OH^- + \frac{1}{2}H_2 \qquad \text{(Equation 2)}$$

With this process, the anodic electrocatalytic aldehyde oxidative dehydrogenation plays a vital role. Typically, Group 11 metals such as Cu, Ag and Au[14] are desired for the low-potential formaldehyde electro-oxidative dehydrogenation reaction since their weak metal-hydrogen (M-H) binding energy is favorable for the hydrogen evolution ($2H^* \rightarrow H_2$, Tafel step) rather than the oxidation of H* that may easily take place on Pt group metals ($H^* + OH^- \rightarrow H_2O - 1e^-$). Among the Group 11 metals, Cu is particular attractive for its earth-abundance and low cost. However, monometallic Cu electrocatalysts often exhibit limited activity and stability, leading to rapid performance decay.[10, 15] Therefore, the anode electrocatalyst development remains to be a limiting challenge in this field. To this end, a number of bimetallic electrocatalysts, including CuAg[9, 16], CuAu[17], CuPd[17] and CuPt[17] have been explored to improve the performance and durability of Cu-based electrocatalysts. However, the introduction of these precious metals leads to substantial cost increase (over 2 order of magnitudes) compared with Cu.[18] and the hydrogen spillover and oxidation (e.g., in the case of CuPt) also could substantially lower the FE of anodic hydrogen evolution.[17]

It has been suggested that formaldehyde oxidative dehydrogenation typically involves the adsorption of hydroxy methoxide anion ($H_2CO + OH^- \rightarrow H_2C(OH)O^-$) followed by $1e^-$ oxidation that leads to M-H bond formation and adsorbed formate.[16] Therefore,

electrocatalysts that can facilitate the hydrogen production (2H*→H_2, Tafel step) and formate desorption is beneficial for the formaldehyde oxidative dehydrogenation. Based on the volcano plot, Sn has further lowered M-H binding energy compared with Cu,[19-20] indicating it could further facilitate hydrogen desorption for anodic hydrogen production. In addition, CuSn alloy has also been widely reported as CO_2 reduction reaction (CO_2RR) electrocatalysts with formate as the main product,[21-23] suggesting that the CuSn alloy could also facilitate the formate desorption upon the introduction of Sn.[16] Therefore, we designed and synthesized noble metal free Cu_6Sn_5 alloy electrocatalysts via a facile electrodeposition method, achieving an ultrahigh current density of 915±46 mA/cm^2 at 0.4 V vs. reversible hydrogen electrode (RHE) for formaldehyde electro oxidative dehydrogenation. Furthermore, using Cu_6Sn_5 alloy as the anode electrocatalysts, the formaldehyde assisted water electrolyser delivers a current density of 100 mA/cm^2 at a low voltage of 0.124 V and a high current density of 486±20 mA/cm^2 at 0.6 V without any iR compensation, and retains a stable nearly 200% combined FE for both anodic and cathodic hydrogen production while concurrently converting formaldehyde into value-added formate during 88 hours of continued operation. Density functional theory (DFT) calculations confirms that the Cu_6Sn_5 surface can facilitate the $H_2C(OH)O^-$ adsorption, promote the dehydrogenation, *H recombination and formate desorption, offering advantages in reaction kinetics and reduced susceptibility to site poisoning.

2 Results and discussion

2.1 Synthesis and Characterization

The CuSn electrocatalysts were synthesized via a hydrogen bubble template electrodeposition method with $CuSO_4$ and $SnSO_4$ as the precursors, respectively. The structural characterizations of the as-prepared Cu_6Sn_5 electrocatalysts demonstrate branched shape morphology and Cu_6Sn_5 alloy phase as shown in Figure S1-S3. Regarding the Cu_6Sn_5

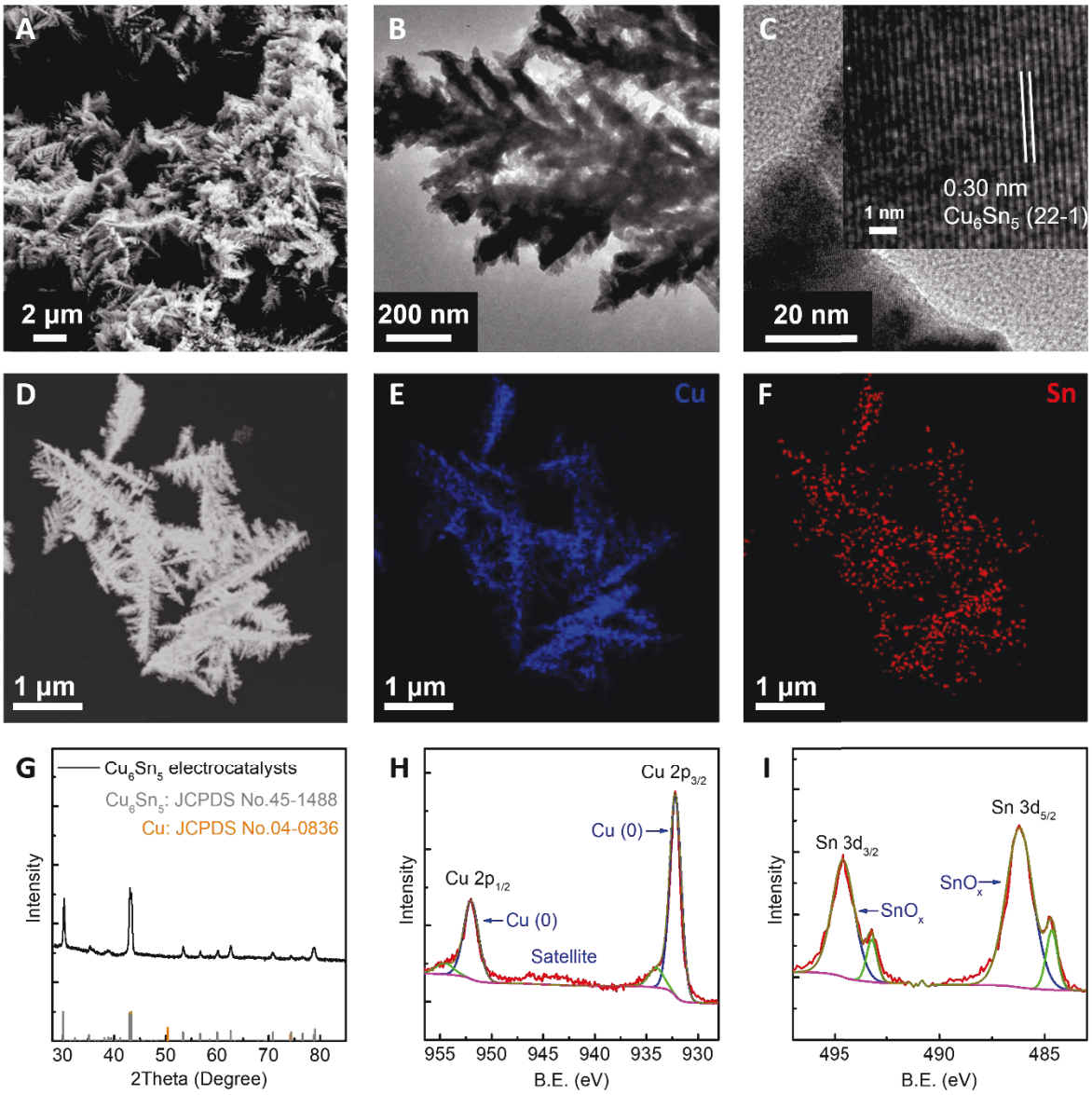

Figure 1. Structural characterizations of the Cu_6Sn_5 electrocatalysts under working conditions. (A) SEM image of Cu_6Sn_5 electrocatalysts. (B) TEM image of Cu_6Sn_5 electrocatalysts. (C) HRTEM image of Cu_6Sn_5 electrocatalysts. (D) STEM image of Cu_6Sn_5 electrocatalysts. (E) EDX mapping of Cu_6Sn_5 electrocatalysts (Cu element). (F) EDX mapping of Cu_6Sn_5 electrocatalysts (Sn element). (G) XRD pattern of Cu_6Sn_5 electrocatalysts. (H) XPS study of Cu_6Sn_5 electrocatalysts (Cu 2p). (I) XPS study of Cu_6Sn_5 electrocatalysts (Sn 3d).

electrocatalysts after 10-hour electrochemical testing, scanning electron microscopy (SEM) and transmission electron microscopy (TEM) pictures demonstrate branched-pine shape morphology (Figure 1A and 1B). The high-resolution TEM (HRTEM) shows a well-resolved lattice spacing of 0.30 nm (Figure 1C) corresponding to the (22-1) facet of the monoclinic η'-

Cu_6Sn_5 alloy.[24-25] Energy dispersive X-ray spectroscopy (EDX) mapping demonstrates the uniform distribution of the Cu and Sn elements (Figure 1D, 1E and 1F). The X-ray diffraction (XRD) pattern confirms the η'-Cu_6Sn_5 alloy, which represents the most stable alloy phase formed between Cu and Sn under room temperature[26] and consistent with studies under similar conditions.[24-25] X-ray photoelectron spectroscopy (XPS) demonstrates that Cu is mostly in Cu^0 state while surficial Sn exists mostly in the oxidized form (SnO_x) potentially attributed to air exposure.[24] For comparison, the Cu electrocatalyst with a similar branched morphology was also synthesized under similar condition with (111) facet exposed (Figure S4).[27]

2.2 Single electrode test

The electrochemical properties of the Cu_6Sn_5 alloy electrocatalysts were studied in a single compartment electrochemical cell, with Hg/HgO reference electrode and graphite counter electrode. We first conducted linear scan voltammetry (LSV) to evaluate the performance of the Cu_6Sn_5 alloy electrocatalysts for formaldehyde oxidative dehydrogenation. The LSV shows that the Cu_6Sn_5 alloy electrocatalysts demonstrate a high current density of 315±16 mA/cm^2 at 0.4 V vs. RHE even without iR compensation, which is considerably higher than that of Cu electrocatalysts (123±6 mA/cm^2 at 0.4 V vs. RHE) (Figure 2A). By implementing an 80% iR compensation due to the ultrahigh current density in the higher potential region (Figure S5), the Cu_6Sn_5 alloy electrocatalyst deliver an ultrahigh current density of 915±46 mA/cm^2 at 0.4 V vs. RHE (Figure 2B), which is nearly 6-fold improvement compared with Cu electrocatalysts (144±8 mA/cm^2 at 0.4 V vs. RHE). Such notable performance improvement is likely arisen from the synergy between Cu and Sn. In particular, the introduction of Sn could facilitate the Tafel step for H* species desorption and hydrogen evolution (*H+*H→H_2) during the formaldehyde electro oxidative dehydrogenation because of the weakened M-H binding energy of Sn according.[19-20] Additionally, CuSn alloy

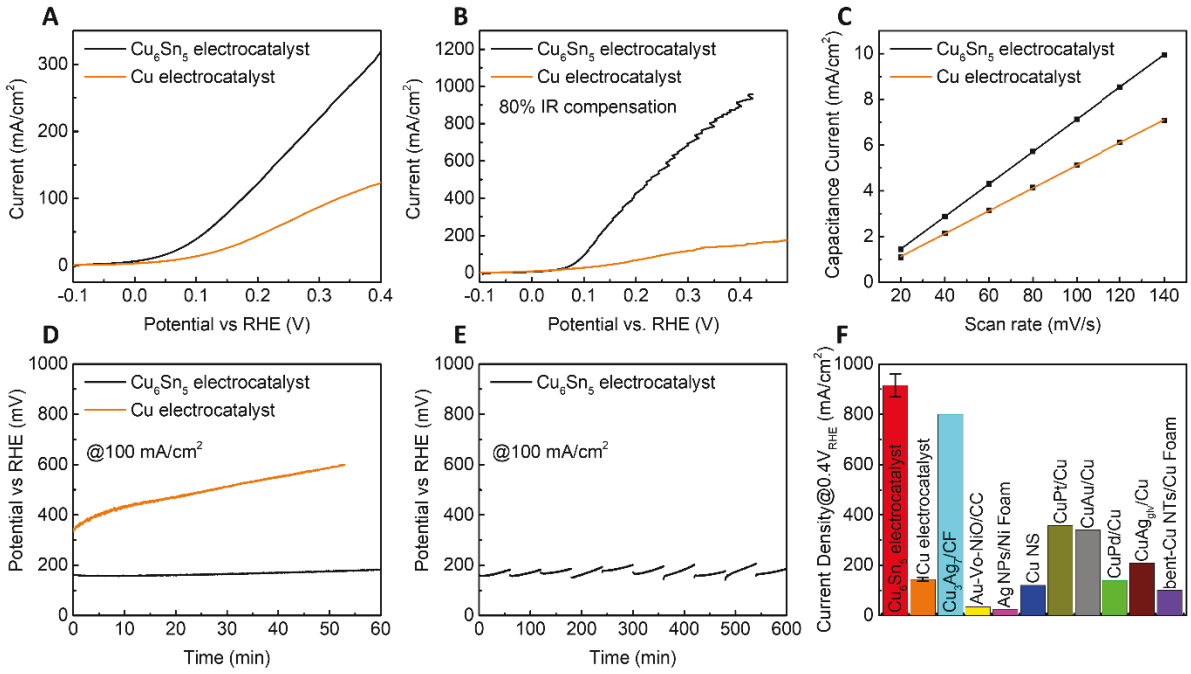

Figure 2. Single electrode test of Cu_6Sn_5 and Cu electrocatalysts. (A) LSV polarization curves of Cu_6Sn_5 and Cu electrocatalysts. (B) LSV polarization curves with 80% IR compensation. (C) Linear fitting of the double layer capacitance current from scan rate of 20 mV/s to 140 mV/s. (D) CP test of Cu_6Sn_5 and Cu electrocatalysts at 100 mA/cm^2. (E) Cumulative CP tests of Cu_6Sn_5 electrocatalysts at 100 mA/cm^2 for 10 hours. (F) Summary and comparison with previously reported aldehyde electro oxidative dehydrogenation electrocatalysts.

electrocatalysts[21-22] and their counterpart with surficial oxides (*e.g.* $CuSn/SnO_x$)[23] has also been reported for CO_2RR to formate, indicating that the Sn species could be favorable for formate desorption that is also important for formaldehyde electro oxidative dehydrogenation.

We have also tested the performance on the electrodeposited Sn and found no appreciable catalytic performance for formaldehyde oxidative dehydrogenation (Figure S6). Furthermore, Sn showed notable self-electrooxidation, with the current rapidly decaying and Sn severely falling off from the electrode over each LSV scan (Figure S6). In contrast, the LSV curve of Cu_6Sn_5 alloy showed negligible current in the electrolyte without formaldehyde, indicating little self-electrooxidation of Sn in the Cu_6Sn_5 alloy (Figure S7). These studies and further confirm the indispensable roles of both Cu and Sn for robust formaldehyde electro-oxidative dehydrogenation.

We further evaluated the electrochemical surface area (ECSA) by conducting the electric double layer capacitance measurements at different scan rates from 20 mV/s to 140 mV/s (Figure 2C and Figure S8). The Cu_6Sn_5 alloy electrocatalysts demonstrated an ECSA of 34.9±1.0 mF/cm^2, ~1.5 times enhancement compared with the Cu electrocatalysts (24.4±1.3 mF/cm^2), which also generally agrees with the morphology due to comparably fine structure. Thus, the moderate difference in ECSA (<50 %) alone cannot explain the much more significant performance enhancement (~6-fold), suggesting the improvement mostly stems from the synergy between Cu and Sn in the alloy.

We have also conducted chronopotentiometry (CP) tests to evaluate the long-term performance of the electrocatalysts. Impressively, the Cu_6Sn_5 alloy electrocatalysts demonstrates much improved long-term performance with only ~20 mV increase in required potential after 1 h CP test. In sharp contrast, Cu electrocatalysts show much more rapid performance decay with an evident ~300 mV increase within the same period (Figure 2D). In addition, the performance is also generally recoverable by refreshing the electrolyte (Figure 2E), suggesting the slightly reduced performance in CP testing may be attributed to formaldehyde consumption. Our studies further show that the formate itself will not be further oxidized by the electrocatalysts (Figure S9), which is in good agreement with previous report,[16] indicating formate was achieved selectively as a value added product.

We further collected and measured the hydrogen gas produced from both working and counter electrodes during the CP test via the water displacement method (*e.g.,* 1st, 3rd and 9th CP test in Figure S10). Here the formaldehyde electro oxidative dehydrogenation proceeds on the working electrode with Cu_6Sn_5 electrocatalysts (Equation 1), while the hydrogen evolution reaction taking place on the graphite counter electrode (Equation 2), with hydrogen being produced on both electrodes. The overall experimentally collected hydrogen gas volume

agrees well with the theoretical value, indicating a combined 200% faradaic efficiency for hydrogen production. Graphite rod were specifically chosen as the counter electrode in this scenario because Pt could also catalyze the hydrogenation reaction of aldehyde,[28-29] which lowers the cathodic FE for HER. The dissolution of the electrocatalysts were also studied, for example, less than 60 μg Sn dissolution and negligible Cu dissolution (<1 μg) were found during 8-10th CP test, indicating limited Sn dissolution (in agreement with Figure S7), which has negligible impact on the FE measurement for hydrogen production (<0.03 %).

Finally, we compared the performance of our electrocatalysts with previous reports of aldehydes electro-oxidative dehydrogenation processes (Figure 2F). Our Cu_6Sn_5 alloy electrocatalysts not only outperforms Cu electrocatalysts synthesized under similar condition with 6-fold performance enhancement, but also outperforms the previously reported electrocatalysts, including Cu_3Ag_7 on copper foam (Cu_3Ag_7/CF)[16], Au on NiO with O vacancy/carbon cloth (Au-Vo-NiO/CC)[30], Ag nanoparticles on L-arginine etched Ni Foam (Ag NPs/Ni Foam)[31], Cu nanosheet arrays (Cu NS)[15], CuPt/Cu[17], CuAu/Cu[17], CuPd/Cu[17], CuAg catalyst from the galvanic replacement on Cu Foam ($CuAg_{glv}$/Cu)[9], bent Cu nanotube grown on Cu Foam (bent-Cu NTs/Cu Foam)[32] in terms of the current density at 0.4 V vs. RHE. This is particularly significant considering our Cu_6Sn_5 alloy electrocatalyst consists of only low-cost metals without any noble metals such as Ag, Au, Pt, Pd, etc., which is desirable for reducing the electrocatalysts costs.

2.3 Formaldehyde assisted water electrolysis for bipolar hydrogen production

We have further constructed a formaldehyde assisted water electrolyser by combining the anodic formaldehyde oxidative dehydrogenation and cathodic hydrogen evolution together in a membrane electrode assembly (MEA) for bipolar hydrogen production, with Cu_6Sn_5 electrocatalysts and commercial PtNi/C as anode and cathode electrocatalysts, respectively.

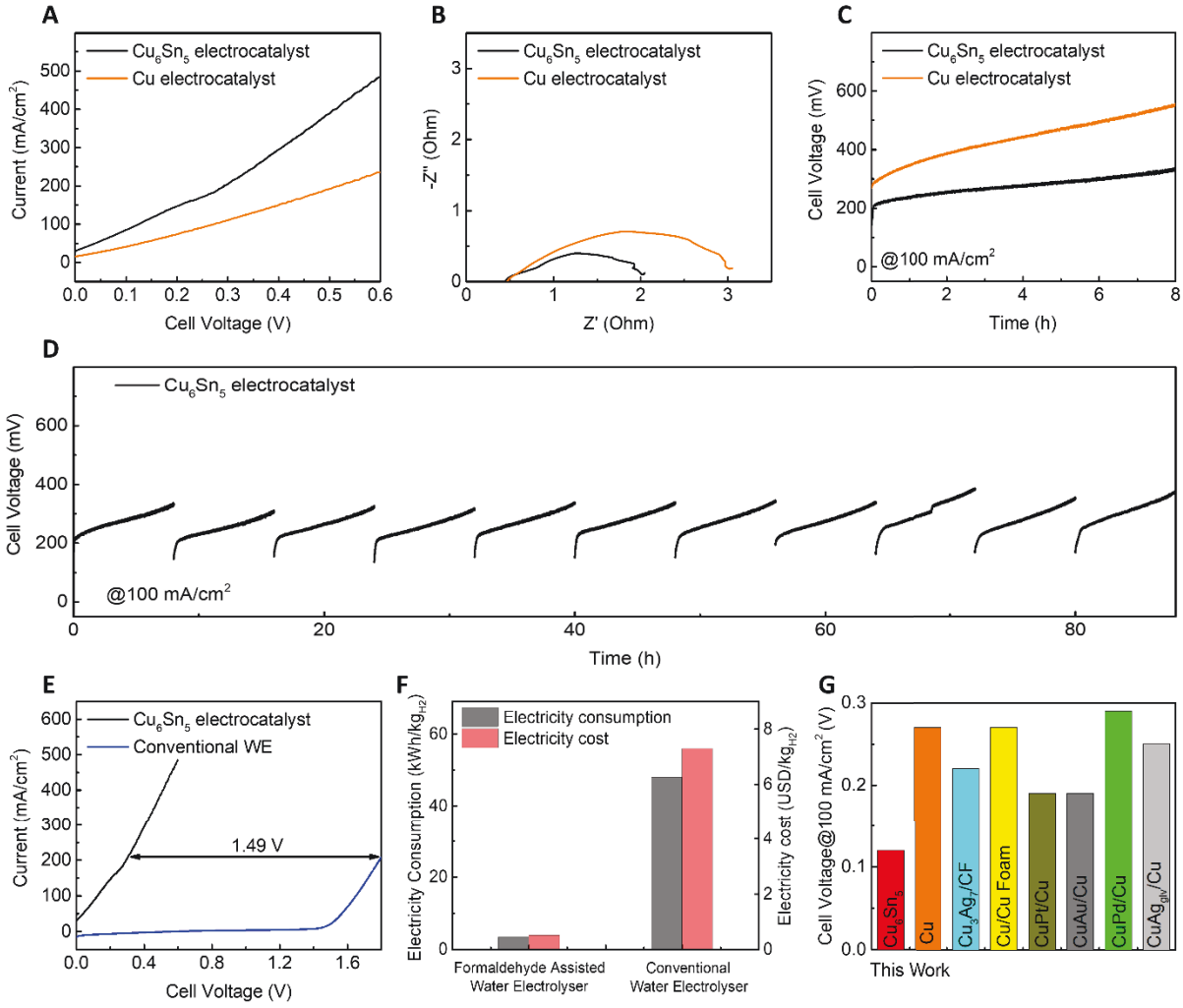

Figure. 3 Formaldehyde assisted water electrolyser test. (A) LSV polarization curves of the electrolyser with Cu_6Sn_5 and Cu employed as anode electrocatalysts. (B) EIS results of the electrolysers. (C) CP tests of the electrolysers at current density of 100 mA/cm^2. (D) Cumulative CP tests of the electrolysers with Cu_6Sn_5 as anode electrocatalysts at current density of 100 mA/cm^2. (E) Comparisons of the polarization curves of formaldehyde assisted water electrolyser with conventional water electrolyser. (F) Comparison of electricity consumption and cost between formaldehyde assisted water electrolyser and conventional water electrolyser at a hydrogen production rate of 3.73 mmol/(h·cm^2) (G) Performance comparison with the previously reported state-of-the-art aldehyde assisted water electrolysers regarding cell voltage at 100 mA/cm^2.

Our MEA-type formaldehyde assisted water electrolyser demonstrates outstanding performance, achieving a current density of 100 mA/cm^2 at an ultralow input voltage of 0.124 V and delivering a high current density of 486±20 mA/cm^2 at 0.6 V (Figure 3A), which far outperforms the counterpart with Cu anode electrocatalyst (100 mA/cm^2 at 0.274 V and

240±11 mA/cm^2 at 0.6 V). Electrochemical impedance spectroscopy (EIS) study demonstrates a low resistance of ~0.45 Ohm, which is essential for achieving the high performance without any iR compensation (the polarization curves after 90% iR compensation are shown in Figure S11). In addition, the charge transfer resistance of the electrolyser implementing Cu_6Sn_5 electrocatalysts (1.5 Ohm) is also lower than that with Cu electrocatalysts (2.5 Ohm), which is consistent with the improved performance (Figure 3B).[33] The Cu_6Sn_5 electrocatalysts || PtNi/C electrolyser also shows considerably more stable performance than the Cu electrocatalysts || PtNi/C electrolyser, with more than 0.1 V lower required voltage to maintain 100/cm^2 current density and only around 25 mV/h performance decay (Figure 3C). Notably, the CP performance is also recoverable upon refreshing the electrolyte after each 8-hour CP test, indicating the consumption of formaldehyde as the main reason the gradual voltage increase. Overall, our formaldehyde assisted water electrolyser could work at 100 mA/cm^2 for 88 hours and show little performance decay with only around 40 mV increase in cell voltage by comparing the 1st and 11th 8-hour test (Figure 3D).

We further analyzed the product during electrolysis. The hydrogen production from anodic and cathodic compartment were collected via water displacement method, demonstrating FE of nearly 100% anode and cathode H_2 production, respectively (Figure S12). ^{1}H NMR test reveals the formate concentration of ~0.58 M after 8 h of CP testing, indicating the conversion of formaldehyde into formate via the electro oxidative dehydrogenation. The electrocatalysts also generally maintained the branched morphology with η'-Cu_6Sn_5 alloy phase, although minor peak from Cu also observed as a result of dealloying due to the Sn dissolution after long term operation (Figure S13 and S14).

We also compared the performance with conventional water electrolyzed (WE) with commercial IrO_x and commercial PtNi/C as the anode and cathode electrocatalysts, respectively. Our formaldehyde assisted water electrolyser demonstrates a decrease of 1.49 V

in cell voltage requirement (Figure 3E) with a combined FE of ~200%, which can lead to substantial energy saving hydrogen production. For example, by considering a hydrogen production rate of 3.73 mmol/(h·cm^2), which is equivalent to 200 mA/cm^2 in conventional water electrolyser or 100 mA/cm^2 in bipolar hydrogen production, the electricity consumption for formaldehyde assisted water electrolyser is only 3.32 kWh per kg H_2 production, which is less than 1/10 of conventional water electrolyser (47.9 kWh per kg H_2 production), leading to a significant saving in electricity cost of 6.78 USD per kg H_2 production (assuming the industrial electricity price of $0.152/kWh in California) (Figure 3F) and could help achieve the DOE target of lowering the cost of hydrogen production to less than 1 USD per kg H_2 production. Furthermore, by utilizing the formaldehyde present in industrial wastewater,[11] our process could facilitate the conversion of waste formaldehyde into formate of higher value. Specifically, the potassium formate has a commodity price of 850 USD/ton (Ex-Shandong), which is more than 4-fold valuable compared with formaldehyde (192 USD/ton, Ex-Shandong).[13]

Finally, we also compared the required cell voltage at current density of 100 mA/cm^2 with those of the previously reported state-of-the-art aldehyde assisted water electrolyser, including Cu_3Ag_7/CF[16], Cu/Cu Foam[10], CuPt/Cu[17], CuAu/Cu[17], CuPd/Cu[17], and $CuAg_{glv}$/Cu[9] (Figure 3G). Overall, our formaldehyde assisted water electrolyser features the lowerest voltage requirement and much cheaper anode electrocatalysts since the cost of Cu and Sn are more than 2 order of magnitudes cheaper than most noble metals such as Ag, Au, Pt, Pd, etc.

2.4 DFT calculations for mechanistic insights

DFT calculations were conducted to elucidate the high performance of formaldehyde

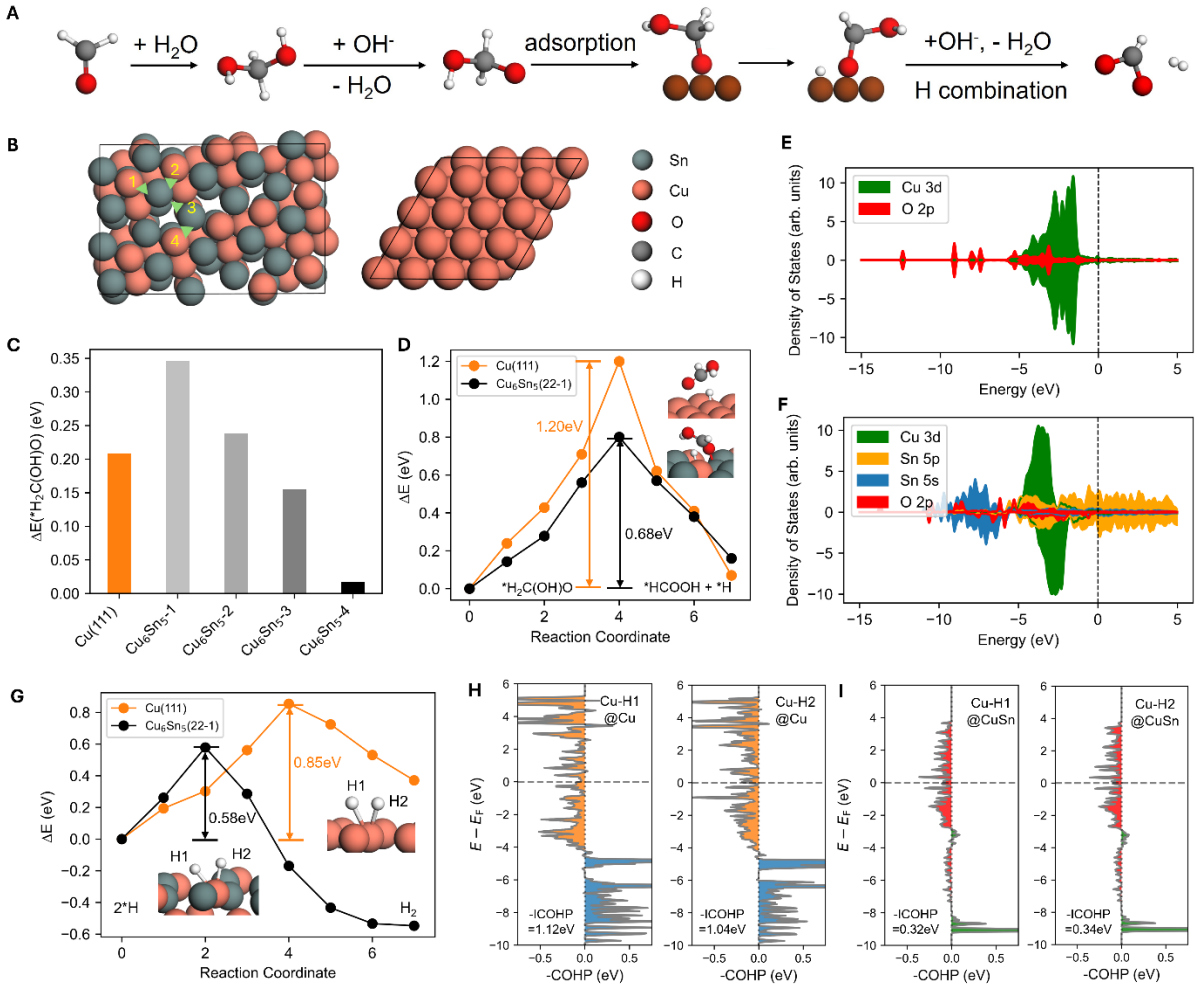

Figure 4. DFT calculations for formaldehyde oxidative dehydrogenation. (A) Schematic representation of proposed reaction pathway. (B) Top view of Cu_6Sn_5(22-1) and Cu(111) surface. (C) Reaction energy of H_2COHOH deprotonation to $H_2C(OH)O^-$ and then adsorption. (D) Reaction trajectories of $H2C(OH)O^-$ dehydrogenation on Cu(111) and Cu_6Sn_5(22-1). (E) Projected density of states of the O atom of $H_2C(OH)O$ and the Cu atom on Cu(111). (F) Projected density of states of the O atom of $H_2C(OH)O$ and the Cu, Sn atoms on Cu_6Sn_5(22-1) (site4). (G) Reaction trajectories of 2*H combination to form H_2 on Cu(111) and Cu_6Sn_5(22-1) surfaces. (H) Crystal orbital Hamilton population (COHP) curves for bond between Cu and H in the transition state of H combination on Cu(111). (I) Crystal orbital Hamilton population (COHP) curves for bond between Cu and H in the transition state of H combination on Cu_6Sn_5(22-1).

oxidative dehydrogenation on Cu_6Sn_5. Based on the experimental observations, Cu(111) and Cu_6Sn_5(22-1) surfaces were selected as model systems (Figure 4B). Figure 4A illustrates the proposed mechanism for formaldehyde oxidative dehydrogenation. Initially, formaldehyde is hydrated and deprotonated in the alkaline media, yielding the $H_2C(OH)O^-$ anion. This anion

is adsorbed onto the catalyst surface, where it undergoes dehydrogenation to form surface-bound *HCOOH and *H species. The HCOOH subsequently undergo oxidation to form formate, while the *H species combine via a Tafel step to release H_2. An effective catalyst should therefore effectively adsorb $H_2C(OH)O^-$, promote its dehydrogenation, and facilitate *H recombination to minimize surface poisoning.

The adsorption of $*H_2C(OH)O$ represents a critical initial step in the dehydrogenation process, as it reflects the substrate's ability to activate and stabilize key intermediates. To this end, we examined the reaction energy for the deprotonation of H_2COHOH to $*H_2C(OH)O$ on Cu(111) and Cu_6Sn_5(22-1). As shown in Figures 4B and 4C, we evaluated four possible adsorption sites for $*H_2C(OH)O$ on the Cu_6Sn_5(22-1) surface. Among these, the bridge site between Cu and Sn atoms (site 4) exhibited the strongest adsorption, while adsorption on the bridge site between two Sn atoms was significantly less favorable. Furthermore, $*H_2C(OH)O$ adsorption was found to be much stronger on the Cu_6Sn_5(22-1) surface compared to the hollow site on Cu(111). Analysis of the projected density of states (PDOS) for the anchored O group of $*H_2C(OH)O$ at the Cu_6Sn_5(22-1) site reveals strong orbital mixing between O 2p states and Cu 3d states from −5 to −1 eV, as well as with Sn 5p and 5s states in the ranges of −1 to 0 eV and −10 to −5 eV (Figure 4F). In contrast, on the Cu(111) surface, only Cu 3d states couple with the O 2p states(Figure 4E). The presence of additional Sn s and p states in the Cu_6Sn_5 alloy leads to enhanced orbital overlap with the O 2p states, contributing to the significantly stronger adsorption energy observed on Cu_6Sn_5(22-1).

The C–H bond cleavage, a critical step in the dehydrogenation process, is illustrated in Figure 4D. The Cu_6Sn_5(22-1) surface exhibits a substantially lower reaction barrier of 0.68 eV compared to the Cu(111) surface, where the barrier reaches 1.2 eV. This indicates that dehydrogenation is significantly more kinetically unfavorable on Cu(111). In the transition state, the O atom in *HCOOH binds with a Sn atom on the Cu_6Sn_5(22-1) surface, whereas

*HCOOH remains physisorbed on the Cu(111) surface. The stronger oxophilicity and lower coordination of Sn on Cu_6Sn_5(22-1) help stabilize the transition state, thereby lowering the reaction barrier. Following the dehydrogenation step, the adsorbed *H species recombine to form H_2 gas, a process commonly known as the Tafel step. Our calculations reveal that the recombination of *H is more facile on Cu_6Sn_5(22-1), with a reaction barrier of 0.58 eV, compared to 0.85 eV on the Cu(111) surface. This indicates that H_2 formation is more kinetically sluggish on Cu(111) (Figure 4G). In this recombination step, *H-H binds to Cu sites on both Cu(111) and Cu_6Sn_5(22-1). Crystal Orbital Hamilton Population (COHP) analysis of the Cu–H bond reveals that Cu on the Cu_6Sn_5(22-1) surface binds *H much more strongly than Cu on the Cu(111) surface (Figure 4H and I). Bader charge analysis reveals a partial electron transfer from Sn to Cu, resulting in a charge-rich state for Cu ($0.23e^-$). This charge accumulation on Cu contributes to the stabilization of the *H-H transition state. This finding further supports the conclusion that the Cu_6Sn_5(22-1) surface is more active for hydrogen evolution than the pure Cu(111) surface.

3 Conclusion

In conclusion, we have designed and synthesized noble metal free Cu_6Sn_5 alloy electrocatalyst via a facile electrodeposition method. The resulting Cu_6Sn_5 alloy exhibits excellent electrocatalytic activity for formaldehyde electro-oxidative dehydrogenation reaction, achieving an ultrahigh geometric current density of 915mA/cm^2 at 0.4 V vs. RHE. Using the Cu_6Sn_5 alloy as formaldehyde dehydrogenation catalyst, we further constructed formaldehyde-assisted water electrolyser with outstanding performance (486 mA/cm^2 at 0.6 V and 0.124 V at 100 mA/cm^2 without any iR compensation) and durability, surpassing previous reports. DFT study reveals that the Cu_6Sn_5(22-1) surface exhibits superior performance across all key steps of the reaction mechanism—$H_2C(OH)O^-$ adsorption, C–H bond cleavage, and *H recombination—compared to Cu(111). This work presents an effective

path for developing noble metal free, low cost electrocatalysts for formaldehyde oxidative dehydrogenation reaction. It could enable formaldehyde assisted water electrolysis for cost-effective bipolar hydrogen production along with effective chemical upgrading.

Acknowledgements

X.D. and Y.H. are grateful for the gracious support from NewHydrogen, Inc. D.C. and P.S. acknowledge support from the National Science Foundation award 2103116. D. C. used the HOFFMAN2 cluster at the UCLA Institute for Digital Research and Education (IDRE) and the Expanse cluster through the allocation CHE170060 at the San Diego Supercomputing Center through ACCESS.

Conflict of Interest

The authors declare no conflict of interest.

References

[1] X. Fu, C. Wan, H. Huyan, S. Wang, A. Zhang, J. Zhou, H. Zhang, X. Zhao, J. Chen, X. Pan, Y. Huang, X. Duan, *EES Catalysis* **2024**, *2*, 1285-1292.
[2] Z. Li, Y. Yan, S.-M. Xu, H. Zhou, M. Xu, L. Ma, M. Shao, X. Kong, B. Wang, L. Zheng, H. Duan, *Nature Communications* **2022**, *13*, 147.
[3] X. Fu, D. Cheng, A. Zhang, J. Zhou, S. Wang, X. Zhao, J. Chen, P. Sautet, Y. Huang, X. Duan, *Energy Environmental Science* **2024**, *17*, 2279-2286.
[4] Q. Mao, X. Mu, K. Deng, H. Yu, Z. Wang, Y. Xu, X. Li, L. Wang, H. Wang, *ACS Nano* **2022**, *17*, 790-800.
[5] Y. Sun, H. Shin, F. Wang, B. Tian, C.-W. Chiang, S. Liu, X. Li, Y. Wang, L. Tang, W. A. Goddard III, M. Ding, *Journal of the American Chemical Society* **2022**, *144*, 15185-15192.
[6] S.-K. Geng, Y. Zheng, S.-Q. Li, H. Su, X. Zhao, J. Hu, H.-B. Shu, M. Jaroniec, P. Chen, Q.-H. Liu, *Nature Energy* **2021**, *6*, 904-912.
[7] J.-T. Ren, L. Chen, H.-Y. Wang, W.-W. Tian, Z.-Y. Yuan, *Energy & Environmental Science* **2024**, *17*, 49-113.
[8] H. Y. Wang, M. L. Sun, J. T. Ren, Z. Y. Yuan, *Advanced Energy Materials* **2023**, *13*, 2203568.
[9] H. Liu, N. Agrawal, A. Ganguly, Y. Chen, J. Lee, J. Yu, W. Huang, M. M. Wright, M. J. Janik, W. Li, *Energy & Environmental Science* **2022**, *15*, 4175-4189.
[10] T. Wang, L. Tao, X. Zhu, C. Chen, W. Chen, S. Du, Y. Zhou, B. Zhou, D. Wang, C. Xie, P. Long, W. Li, Y. Wang, R. Chen, Y. Zou, X.-Z. Fu, Y. Li, X. Duan, S. Wang, *Nature Catalysis* **2022**, *5*, 66-73.
[11] A. Hidalgo, A. Lopategi, M. Prieto, J. Serra, M. Llama, *Applied Microbiology and biotechnology* **2002**, *58*, 260-264.
[12] H. R. Lotfy, I. Rashed, *Water Research* **2002**, *36*, 633-637.

[13] D. A. Bulushev, J. R. Ross, *ChemSusChem* **2018**, *11*, 821-836.
[14] J. Van Den Meerakker, *Journal of Applied Electrochemistry* **1981**, *11*, 387-393.
[15] Y. Yang, X. Wu, M. Ahmad, F. Si, S. Chen, C. Liu, Y. Zhang, L. Wang, J. Zhang, J. L. Luo, *Angewandte Chemie International Edition* **2023**, *62*, e202302950.
[16] G. Li, G. Han, L. Wang, X. Cui, N. K. Moehring, P. R. Kidambi, D.-e. Jiang, Y. Sun, *Nature Communications* **2023**, *14*, 525.
[17] H. Liu, J. Yu, Y. Chen, J. Lee, W. Huang, W. Li, *ACS Applied Materials & Interfaces* **2023**, *15*, 37477-37485.
[18] X. Fu, C. Wan, Y. Huang, X. Duan, *Advanced Functional Materials* **2022**, *32*.
[19] B. Conway, G. Jerkiewicz, *Electrochimica Acta* **2000**, *45*, 4075-4083.
[20] M. Jaksic, *Journal of New Materials for Electrochemical Systems* **2000**, *3*, 153-168.
[21] B. Ning, W. Chang, M. Liu, H. Jiang, C. Li, *ChemElectroChem* **2021**, *8*, 1150-1155.
[22] J. Wang, J. Zou, X. Hu, S. Ning, X. Wang, X. Kang, S. Chen, *Journal of Materials Chemistry A* **2019**, *7*, 27514-27521.
[23] K. Ye, Z. Zhou, J. Shao, L. Lin, D. Gao, N. Ta, R. Si, G. Wang, X. Bao, *Angewandte Chemie International Edition* **2020**, *59*, 4814-4821.
[24] J. Shao, H. Jing, P. Wei, X. Fu, L. Pang, Y. Song, K. Ye, M. Li, L. Jiang, J. Ma, *Nature Energy* **2023**, *8*, 1273-1283.
[25] H. C. Shin, M. Liu, *Advanced Functional Materials* **2005**, *15*, 582-586.
[26] J.-H. Shim, C.-S. Oh, B.-J. Lee, D. Lee, *International Journal of Materials Research* **1996**, *87*, 205-212.
[27] S. J. Kim, Y. I. Kim, B. Lamichhane, Y.-H. Kim, Y. Lee, C. R. Cho, M. Cheon, J. C. Kim, H. Y. Jeong, T. Ha, *Nature* **2022**, *603*, 434-438.
[28] R. Hirschl, A. Eichler, J. Hafner, *Journal of Catalysis* **2004**, *226*, 273-282.
[29] S. Zhao, Y. Wen, X. Peng, Y. Mi, X. Liu, Y. Liu, L. Zhuo, G. Hu, J. Luo, X. Tang, *Journal of Materials Chemistry A* **2020**, *8*, 8913-8919.
[30] Z. Li, Y. Zhang, Q. Yang, J. Wu, Z. Ren, F. Si, J. Zhao, J. Chen, *Iscience* **2023**, *26*, 107994.
[31] Y. Zhang, J. Wu, X. Zhu, Z. Ren, J. Chen, *Applied Catalysis B: Environment and Energy* **2024**, *354*, 124093.
[32] T. Wang, Z. Huang, T. Liu, L. Tao, J. Tian, K. Gu, X. Wei, P. Zhou, L. Gan, S. Du, Y. Zou, R. Chen, Y. Li, X.-Z. Fu, S. Wang, *Angewandte Chemie* **2022**, *134*, e202115636.
[33] X. Fu, D. Cheng, C. Wan, S. Kumari, H. Zhang, A. Zhang, H. Huyan, J. Zhou, H. Ren, S. Wang, Z. Zhao, X. Zhao, J. Chen, X. Pan, P. Sautet, Y. Huang, X. Duan, *Advanced Materials* **2023**, *35*, 2301533.